Magnetic phase diagram of Y_2CuO_4: Weak ferromagnetism and metamagnetic transition

A. Rouco and X. Obradors
Institut de Ciència de Materials de Barcelona, Consejo Superior de Investigaciones Científicas, Campus Universitat Autònoma de Barcelona, 08193 Bellaterra, Spain

M. Tovar
Centro Atòmico Bariloche, Comisión Nacional de Energía Atómica and Instituto Balseiro, Universidad Nacional de Cuyo, 8400 San Carlos de Bariloche, Río Negro, Argentina

F. Pérez
Institut de Ciència de Materials de Barcelona, Consejo Superior de Investigaciones Científicas, Campus Universitat Autònoma de Barcelona, 08193 Bellaterra, Spain

D. Chateigner and P. Bordet
Laboratoire de Cristallographie, CNRS, 38042 Grenoble, France
(Received 23 March 1994)

We have studied the magnetic properties of Y_2CuO_4, synthesized at high pressures. This cuprate crystallizes in the Nd_2CuO_4-type structure (T'), characteristic of the electron-doped superconductors. Since the Y ions are nonmagnetic, this compound is very suitable to study the magnetism of the Cu lattice, without any interference from the rare earths. We have measured dc magnetization vs temperature in several magnetic fields up to 50 kOe, both after field cooling (FC) and zero-field cooling (ZFC) the samples, and we have made isothermal magnetization measurements vs field, from 5 to 340 K. We have also performed a detailed study of the ac-susceptibility dependence on the dc field, the ac field, and the frequency. All the measurements indicate a three-dimensional antiferromagnetic (AF) ordering of the Cu lattice below $T_N=257(1)$ K, with the Cu spins slightly canted away from perfect AF alignment. This canting produces a weak ferromagnetic (WF) component for each CuO_2 plane. However, at zero field, the AF coupling between different planes makes that the WF components remain almost compensated, and only after a metamagnetic transition can the weak ferromagnetic behavior be evidenced. Above T_N, the WF component is still induced by the field in a large temperature interval. Below T_N, an irreversibility line has been determined from hysteresis loops and magnetization vs temperature measurements in FC and ZFC conditions. It follows a de Almeida–Thouless law $H_{irr} \propto (T_N - T_{irr})^{3/2}$. Below the irreversibility line, typical logarithmic relaxation processes of the ZFC magnetization are detected. Finally, an activated dynamic scaling describes the frequency dependence of the ac-susceptibility peak found below T_N and associated with magnetic freezing processes. All these features are characteristic of the existence of finite-size weak ferromagnetic clusters.

I. INTRODUCTION

The discovery of superconductivity in the electron-doped compounds $R_{2-x}A_xCuO_4$ (R=Pr, Nd, Sm, Eu; A=Ce, Th),[1] which crystallize in the tetragonal Nd_2CuO_4-type structure (T' phase), has stimulated a number of studies on the magnetic properties of the series of rare-earth cuprates (R_2CuO_4, R=Pr, . . . , Tm, Y) with the same structural phase. Referring to the Cu sublattice, a peculiar characteristic of this structure is the square-planar coordination of the Cu ions which lie in CuO_2 planes.

In Nd_2CuO_4, neutron-scattering experiments have shown a transition from a state with strong two-dimensional antiferromagnetic (AF) correlations to a three-dimensional antiferromagnetic (AF) phase below $\simeq$255 K, with an ordered magnetic moment of $0.4(1)\mu_B$/Cu atom.[2,3] On cooling, two other magnetic phase transitions in which the Cu spins reorient have also been observed. Other transitions affecting only the Nd spins, and not the Cu sublattice, have been detected too. Otherwise, no evidence for a distortion from the T' structure has been observed at any temperature.

In Sm_2CuO_4 and Pr_2CuO_4, neutron-scattering experiments have also indicated a transition to three-dimensional AF order, from a phase with strong two-dimensional AF correlations.[3,4] In these cases, the transition temperatures are 255 and 280 K, the ordered magnetic moments are 0.40 and $0.38\mu_B$/Cu atom, respectively, and no changes occur in the Cu spin sublattice below the transition temperature.

Recently, magnetization measurements on Nd_2CuO_4 single crystals and field-dependent neutron-diffraction measurements on Nd_2CuO_4 and Sm_2CuO_4 single crystals have stated a noncollinear magnetic structure for these two compounds.[5,6] It means that the Cu spins are AF

aligned along the a axis for a CuO_2 plane and along the b axis for its neighboring layers. It has also been pointed out that there is the possibility of the same noncollinear magnetic structure for Pr_2CuO_4.[6]

When these cuprates are doped with Ce or Th, the temperature of the three-dimensional AF ordering continuously decreases until 0 K and, after that, a superconducting phase is achieved.[7] Despite this, Gd_2CuO_4 has also been doped with Ce, but it does not show superconductivity.[8]

In Gd_2CuO_4, a weak peak in the susceptibility at $\simeq 275$ K has been found with the field applied parallel to the CuO_2 planes.[9] Almost no angular dependence within the ab planes has been found, but there is no signal of peak for fields applied perpendicular to these planes. Neutron-diffraction experiments on Gd_2CuO_4 have indicated that, below the temperature of the susceptibility peak, the Cu moments order AF along the $\{110\}$ directions.[10] These features have been tentatively attributed to a transition from a state with two-dimensional AF short-range correlations to a state with three-dimensional AF order with a weak ferromagnetic (WF) component. This component should be due to a canting of the Cu moments out of the $\{110\}$ directions within the CuO_2 planes. It has been proposed that the Dzyaloshinski-Moriya interaction probably produces this canting.[11] This interaction will be canceled unless we assume that the local crystal symmetry is lower than tetragonal, i.e., there is a local distortion of the crystal structure and the Cu-O coordination is no longer square planar.

For the heavier rare-earth cuprates (R = Tb, Dy, Ho, Er, Tm), a transition to three-dimensional AF order with a WF component has also been detected, by means of magnetic measurements.[12]

Several investigations concerning the phase diagram of the cuprates $(GdR)_{1.85}Ce_{0.15}CuO_{4-\delta}$, where R = Pr, Nd, and Sm, have been developed.[7,13] These studies showed that the superconducting behavior in the cuprates without Gd is suppressed with increasing Gd concentration. In this case, a high concentration of Gd produces not only an AF order of the Cu spins, but also a WF component of these spins. As previously discussed, this component may only occur if it is assumed that a local structural distortion reducing the tetragonal symmetry of the compound occurs. In this case, increasing the Gd concentration at the expense of Pr, Nd, or Sm ions generates a displacement of the oxygen atoms within the CuO_2 planes, which leads to a local orthorhombic symmetry, induces the WF component, and suppresses the superconducting behavior. It is still unknown why such a distortion of the CuO_2 planes cannot coexist with superconductivity, but there are several examples which show that there is a close relationship between the crystal symmetry and the superconducting behavior in the layered cuprates.[14]

Knowing the relevance of the Cu sublattice in the physical properties of the layered cuprates, Y_2CuO_4 appears to be an excellent material to study their magnetic properties because the nonmagnetic character of Y^{3+} ions will allow a full study of the magnetic behavior of CuO_2 planes.

In a previous work,[15] we observed a peak at $T_N = 257$ K in the low-field magnetization measurements of Y_2CuO_4, similar to that found for Gd_2CuO_4, and a field-induced transition below T_N, similar to that found for La_2CuO_4.[16] We concluded that a transition to a three-dimensional AF order, with a WF component due to a canting of the Cu moments, occurs at T_N. Below this temperature, a field-induced metamagneticlike transition takes place and, below this transition, the interlayer AF coupling masks the WF order. In this work, we present a detailed study of these transitions and we generate the magnetic phase diagram of the Cu sublattice in Y_2CuO_4, together with an analysis of the complex relationship existing between the magnetic properties and the microstructural features of Y_2CuO_4 oxides.

II. SAMPLE PREPARATION AND STRUCTURAL CHARACTERIZATION

Different samples of Y_2CuO_4 were prepared at high temperature under high pressure using a belt-type apparatus. Two different experimental systems were used, with maximum pressures of 47 and 90 kbar, respectively. The stoichiometric mixture of copper and yttrium oxides was thoroughly ground and heated at 1000 °C for approximately 3 h. This procedure removed hydroxides from the mixture and led to a homogeneous mixture of the intermediate phase $Y_2Cu_2O_5$ and part of the yttrium oxide Y_2O_3. We then sealed this mixture in platinum capsules and we placed them in the high-pressure furnace. The pressure was first increased to different values between 45 and 85 kbar, at a rate of $\simeq 1.5$ kbar/min. Then the temperature was raised up to 750 °C at $\simeq 150$ °C/min and, finally, to 1000 °C at $\simeq 50$ °C/min. Both parameters were kept constant for about 75 min. The temperature was then decreased to room temperature at $\simeq 150$ °C/min and the pressure released.

Nine different samples, prepared at different pressures between 47 and 85 kbar, were measured in this work. Sample A, weighing $\simeq 20$ mg, is the same used in Ref. 15. We also have to remark that the same synthesis process, at 47 kbar, produced the powder sample designated as C and a piece of ceramic sample designated as D. The larger samples (typically $\simeq 350$ mg) were prepared using the 47-kbar apparatus.

We have confirmed the cationic stoichiometry of the Y_2CuO_4 cuprate by energy-dispersive microanalysis made using a Kevex Delta class analyzer installed on a JSM 840-A scanning electron microscope. X-ray powder-diffraction measurements were made with a Guinier camera using Fe K_α radiation. Although the strongest peaks measured for our Y_2CuO_4 samples may be indexed in the $I4/mmm$ space group with the Nd_2CuO_4-type unit cell (known also as T'), a closer analysis revealed the presence of many extra weak reflexions. These extra reflexions indicate the existence of superstructures with lower symmetry. These superstructures have been identified in Ref. 17 for Tm_2CuO_4, Gd_2CuO_4, and Y_2CuO_4. The approximate size of the corresponding supercells are (a)

$a\sqrt{2}\times a\sqrt{2}\times c$, (b) $2a\sqrt{2}\times a\sqrt{2}\times c$, and (c) $2a\sqrt{2}\times 2a\sqrt{2}\times 2c$. The superstructures have also been observed by electron microscopy, often in different grains of the same sample. The most common lattice superstructure observed for Y_2CuO_4 corresponds to $2a\sqrt{2}\times a\sqrt{2}\times c$. We may conclude that the average structure of Y_2CuO_4 is the tetragonal T', with the lattice parameters $a=3.860$ Å and $c=11.72$ Å, although affected by different types of distortions.

We have tried to prepare samples substituting Ce, Ca, and Sr for Y in the T' structure. We prepared mixtures of the corresponding oxides and followed the same process used to obtain the pure yttrium cuprate, with pressures of synthesis as high as 85 kbar. We prepared samples with nominal composition of dopants ranging from 0.025 atoms/f.u. up to 0.2 atoms/f.u. for Ce, and up to 0.1 atoms/f.u. for Sr. In the case of Ca, we prepared a single sample with 0.15 atoms/f.u. The x-ray-diffraction study of these materials showed a constant value of the lattice parameters for the different nominal compositions. This observation suggests that none of the dopants have entered into the T' structure. The absence of Ce and Ca in the Y-rich phase and the segregation of Ce- or Ca-rich phases was confirmed by energy-dispersive microanalysis.

III. EXPERIMENTAL TECHNIQUES

dc magnetization measurements have been carried out in magnetic fields up to 50 kOe in the temperature range from 5 to 340 K, using a Quantum Design superconducting quantum interference device magnetometer. The core diamagnetism of the sample ($\chi_{dia}\simeq -1.1\times 10^{-8}$ emu/g) has been subtracted in all cases.

The ac susceptibility has been measured with a Lake Shore susceptometer from 5 to 300 K, at frequencies ranging from 10 to 1000 Hz, excitation fields from 1 to 10 Oe, and external dc magnetic fields up to 2 kOe.

IV. RESULTS

A. dc magnetization

As we have previously reported in Ref. 15, a pronounced maximum of the low-field dc magnetization, M_{dc}, is observed for sample A at $T_N\simeq 257$ K. Figure 1(a) shows M_{dc}/H vs T, measured at 60 Oe. The value of the magnetization at the maximum is $M_{dc}/H\simeq 4\times 10^{-5}$ emu/g. Below this temperature, substantial differences are observed between measurements made upon warming after field cooling (FC) the sample in the same magnetic field and those made after zero-field cooling (ZFC) the sample. We have measured the temperature dependence of the magnetization for different applied fields between 60 Oe and 50 kOe. Figures 1(a) and 2(a) show the differences found when the system is cooled under FC or ZFC conditions, for several fields up to 10 kOe. Notice the broadening of the ZFC peak and the evolution of the FC measurements with increasing magnetic field. For fields above 35 kOe, there are no differences between ZFC and FC measurements down to 5 K. Figure 2(b) shows the evolution of M_{dc}/H after FC the sample with the magnetic field of the measurement. We may observe that M_{dc} tends to saturate with increasing magnetic field for all the measured range of temperature.

Hysteresis loops from -50 to 50 kOe at different temperatures have also been measured for sample A. Figure 3 shows characteristic loops for temperatures above and below T_N, measured after FC the sample in 50 kOe. Well above T_N, $M_{dc}(H,T)$ is linear with H up to 50 kOe, as seen in Fig. 3(a) for $T=340$ K. At lower temperatures, but still above T_N, the M_{dc} vs H curves show a fast increase of the magnetization at low fields, reaching a saturation regime for high fields. The magnetic field where this regime is reached decreases continuously with decreasing temperature. The saturation regime may be approximately described by the linear equation:

$$M_{dc}(H,T)=M_S(T)+\chi_{d\infty}(T)H\ , \tag{1}$$

where $\chi_{d\infty}(T)=\lim_{H\to\infty}\chi_d(H,T)$ and $\chi_d(H,T)\equiv\partial M_{dc}(H)/\partial H$ is the differential susceptibility. $M_S(T)$

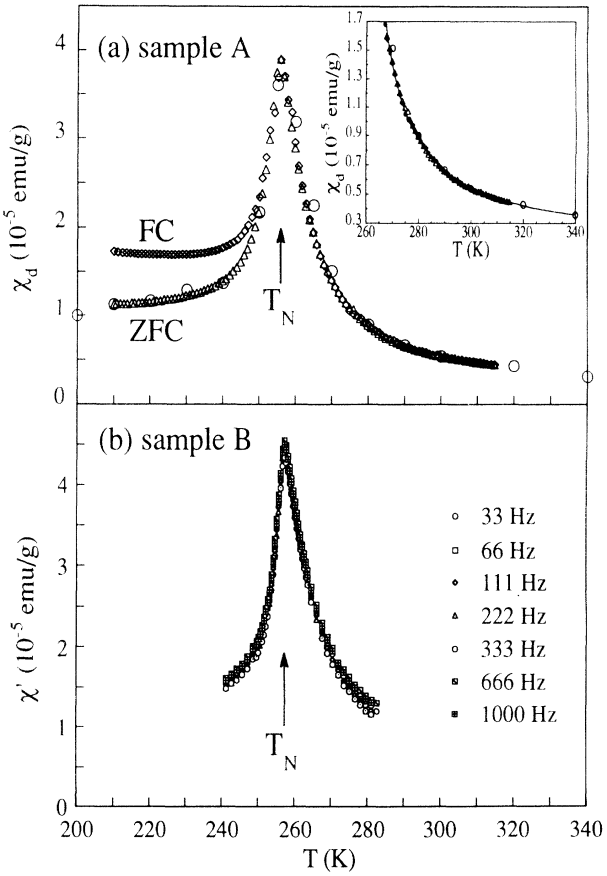

FIG. 1. (a) M_{dc}/H measured for sample A with $H=60$ Oe after field cooling (diamonds) and zero-field cooling (triangles). Circles correspond to the differential susceptibility $\chi_d\equiv\partial M_{dc}/\partial H$ at low fields. Inset: Fit of the high-temperature part of the susceptibility to $\chi_d(T)=\chi_0+(D\chi_0)^2\nu^{-1}(T-T_N)^{-\gamma}$. (b) Real part of the ac susceptibility, $\chi'(T)$, vs temperature measured for sample B with $h_{ac}=5$ Oe and different frequencies between 33 and 1000 Hz.

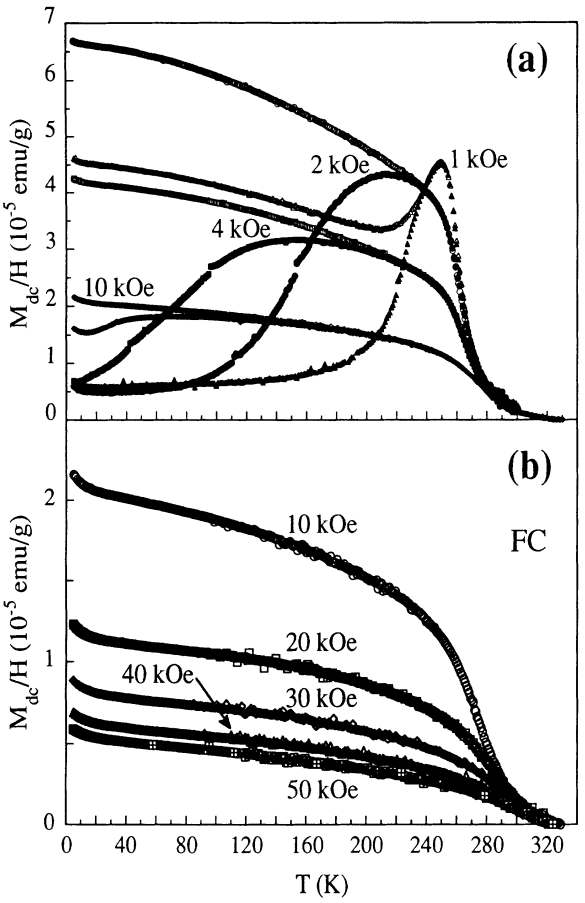

FIG. 2. M_{dc}/H vs T of sample A, (a) measured after ZFC (inferior curves) and FC (superior curves) in 1, 2, 4, and 10 kOe and (b) measured after FC in 10, 20, 30, 40, and 50 kOe.

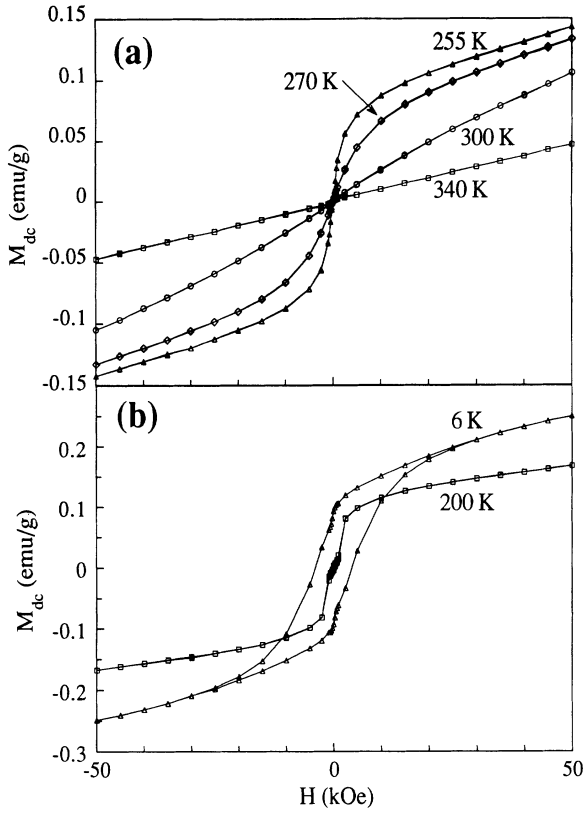

FIG. 3. M_{dc} vs H cycles measured for sample A after FC in 50 kOe (a) above $T_N \approx 255$ K and (b) below T_N. Notice the magnetization jump at $H_c \approx 1$ kOe for $T = 200$ K and the large hysteresis loop at low temperatures.

represents the saturation magnetization extrapolated from the high-field linear regime. At $T=0$, we extrapolate the value $M_S(0) \simeq 9.3 \times 10^{-3} \mu_B$/Cu atom.

Figures 4(a), 4(b), and 4(c) are enlargements of the measured cycles showing the behavior of the magnetization at low fields, at different temperatures below T_N. The M_{dc} vs H curves present a metamagneticlike field-induced transition at a critical field H_c. At low temperatures, the curves show an hysteretic behavior near H_c and around $H=0$ when the magnetic field is reversed in hysteresis loops. In both cases, the hysteresis is strongly dependent on temperature. As seen in Figs. 4(a) and 4(b), $M_{dc}(H)$ is almost linear in the region $-H_c \leq H \leq H_c$. However, at the lowest temperatures, the hysteresis totally masks the intrinsic behavior of this region.

We have also measured magnetization vs field cycles between 0 and 2 kOe, after FC in 2 kOe. A typical cycle is shown in the inset of Fig. 4(a). Due to the hysteretic nature of the transition, two values for the critical fields, H_c' and H_c'', have been determined for increasing and decreasing field measurements, respectively. We have found that these values, shown in Fig. 5 as a function of T, are not dependent on the field used for cooling or on the maximum field reached during the magnetization cycle. Both critical fields coincide at a tricritical point, determined at $T_t \simeq 240$ K and $H_t \equiv H_c(T_t) \simeq 600$ Oe. Above T_t, the $M_{dc}(T)$ vs H curves are reversible when crossing the metamagnetic transition. Below T_t, the metamagnetic transition becomes irreversible and also a hysteresis loop around $H=0$ appears, with a remanent magnetization $M_r \simeq 2.5 \times 10^{-4} \mu_B$/Cu atom. As the temperature decreases, hysteresis develops and H_c'' starts to decrease. For $T \leq 130$ K, H_c'' becomes negative and the hysteresis cycles with two loops centered at $\pm H_c$ gradually become a single loop as the temperature continues to decrease, as shown in Fig. 3(b) for $T=6$ K. As a consequence, this enhancement of the hysteresis produces an abrupt increase of the remanent magnetization.

In order to observe the region below the metamagnetic transition without interferences of the transition or the regime above it, we have measured hysteresis loops between ± 200 Oe at different temperatures below T_N and the first magnetization curves after ZFC at 5 K (Fig. 6) and 180 K, up to fields $H > H_c$. The hysteresis loops between fields lower than H_c are almost reversible and the magnetization vs field is linear from zero field up to H_c at any temperature.

All these dc magnetization measurements were repeated for sample C. The essential results are compared with those of sample A as follows: The maximum of the low-

field dc magnetization vs temperature is only observable after the ZFC procedure; it is located around 200 K and is an order of magnitude larger ($M_{dc}/H \simeq 1.8\times10^{-4}$ emu/g). The differences between ZFC and FC procedures are more pronounced and begin above the temperature of the maximum. The FC measurements do not show a peak, even at low fields; instead, they show a monotonic decrease of the magnetization with increasing temperature. The dc magnetization vs temperature begins to resemble that of sample A for higher fields. The hysteresis loops between ±50 kOe measured after FC sample C in 50 kOe are similar to those of sample A, although the extrapolated saturation magnetization is slightly larger for the whole temperature range of the measurement, $M_S(0)\simeq 11.5\times10^{-3}\mu_B$/Cu atom. The metamagnetic transition can only be observed at low temperatures ($T<60$ K) and, even then, only as a narrowing of the hysteresis loop indicating the existence of two loops centered at $\pm H_c$, similar to that of Fig. 4(c). The first magnetization curve at 5 K after ZFC (Fig. 6) is rather different from that of sample A. In sample C, below the metamagnetic transition located at $H_c' \simeq 5000$ Oe at 5 K, there is a fast increase of the magnetization with field up to $\simeq 2000$ Oe. Between 2000 Oe and H_c', there is a linear saturation regime, with an extrapolated saturation magnetization $M_S(5\ \text{K})\simeq 1.3\times10^{-3}\mu_B$/Cu atom.

We have also measured the dc magnetization vs temperature of sample D, for different fields after ZFC the sample. We show some of these measurements in Fig. 7.

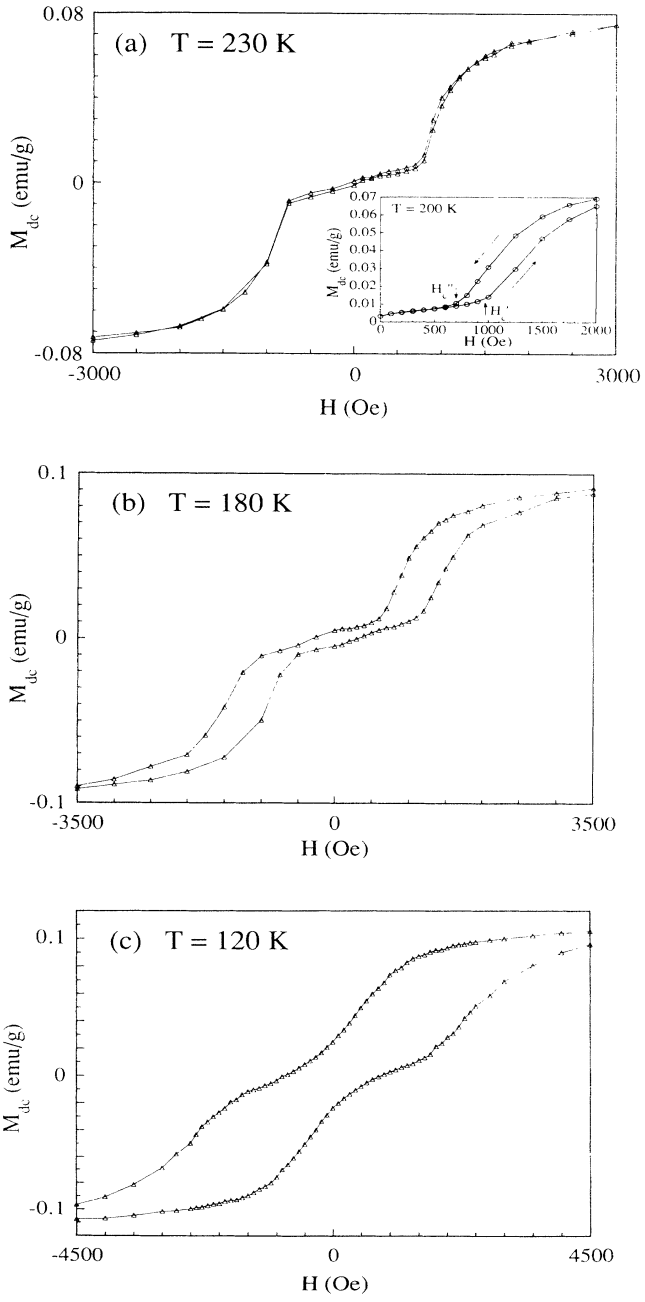

FIG. 4. Enlargement of the central zone of M_{dc} vs H loops between ±50 kOe measured after FC in 50 kOe for (a) 230 K, (b) 180 K, and (c) 120 K. Inset: Magnetization measured at 200 K for a smaller field cycle between 0 and 2 kOe, after FC in 2 kOe. The arrows indicate the definition of H_c' and H_c'' as used in the text.

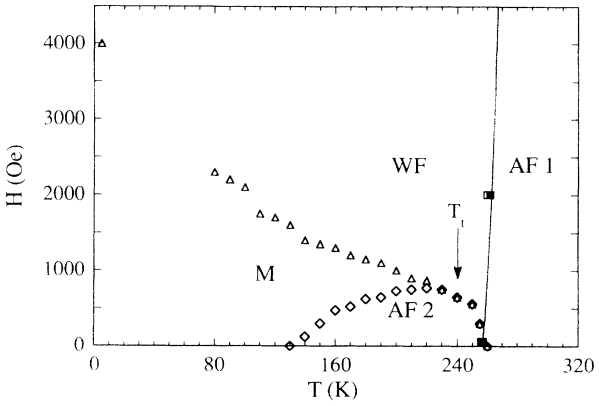

FIG. 5. Phase diagram of sample A of Y_2CuO_4. Triangles and diamonds correspond to the critical fields H_c' and H_c'', respectively. The squares and the solid line determine the WF transition.

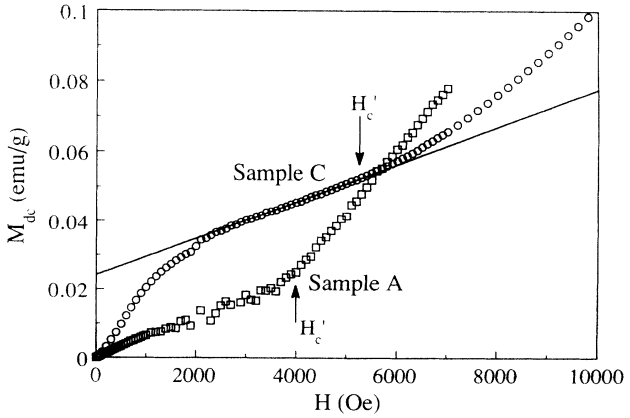

FIG. 6. First magnetization curves measured at 5 K after ZFC for samples A (squares) and C (circles). The linear fit of the saturation magnetization of sample C below H_c is also plotted. The arrows signal H_c' (5 K) for both samples.

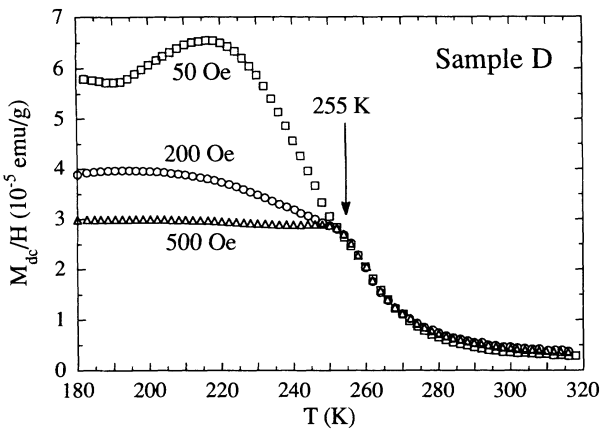

FIG. 7. M_{dc}/H vs T measured at 50 Oe (squares), 200 Oe (circles), and 500 Oe (triangles) after ZFC for sample D. Notice the shoulder at $\simeq 255$ K, which becomes visible for the higher fields.

At low fields ($H=50$ Oe), a peak at $\simeq 217$ K is present, with a value of the magnetization, $M_{dc}/H \simeq 6.5\times10^{-5}$ emu/g, intermediate between those of samples A and C. Increasing the magnetic field, this peak quickly becomes weaker, unmasking a shoulder at about 255 K. The value of the magnetization at this shoulder, $M_{dc}/H \simeq 3\times10^{-5}$ emu/g, is rather similar to the value at the peak of sample A and, consequently, we will relate the shoulder with the peak at $T_N=257(1)$ K.

The low-field dc magnetization of sample E has also been measured as a function of temperature. We have found a peak at $\simeq 185$ K stronger and broader than the peaks found in the other samples. The magnetization at the peak is $M_{dc}/H \simeq 4.5\times10^{-4}$ emu/g. The irreversibility between ZFC and FC measurements begins above the temperature of the maximum and it is very pronounced. In fact, this sample exhibits a peculiar behavior, rather similar to that of sample C.

B. ac susceptibility

At the same temperature of the maximum of the low-field dc magnetization, we have observed a peak in the real component of the ac susceptibility of sample A. The value of the susceptibility at this peak, $\chi'_{max}\simeq 4\times10^{-5}$ emu/g, coincides with the maximum of M_{dc}/H at low field. A detailed analysis of the ac susceptibility was carried out for samples B and C because of its larger size ($m>160$ mg).

We have measured sample B with an excitation field of 5 Oe and different frequencies between 33 and 1000 Hz. All the measurements show a peak at $\simeq 257$ K for the real component of the ac susceptibility with a maximum, $\chi'_{max}\simeq 4\times10^{-5}$ emu/g, very similar to that found in sample A [Fig. 1(b)]. The imaginary component, $\chi''(T)$, also shows a peak at approximately the same temperature. We have not detected any variation with frequency within our experimental sensitivity.

Sample C shows a more intense maximum of both components of the ac susceptibility at $\simeq 220$ K ($\chi'_{max}\simeq 2.5\times10^{-4}$ emu/g). This maximum shows some dependence on the ac field, between 1 and 10 Oe. This field dependence is related to the deviations from linearity in the M_{dc} vs H curves, even at low fields. The frequency dependence for both the real, $\chi'(T)$, and the imaginary, $\chi''(T)$, parts of the ac susceptibility is shown in Fig. 8. Well above the maximum, $\chi'(T)$ is almost frequency independent. Near the susceptibility peak and below it, $\chi'(T)$ is smaller for the higher frequencies. This frequency dependence becomes smaller as the temperature is lowered and no differences between the values for 10 and 1000 Hz were detected below $\simeq 80$ K. $\chi''(T)$ also presents a maximum, although at a temperature somewhat below that of $\chi'(T)$. For temperatures above the maximum, $\chi''(T)$ is reduced for smaller frequencies and, for temperatures below the peak, the frequency dependence is negligible. We have also measured the ac susceptibility of this sample under applied dc magnetic fields up to 2 kOe. With an increase in the dc field applied upon the sample, the susceptibility peak largely broadens and weakens and its maximum shifts towards higher temperature.

The ac susceptibility of sample D also exhibits a maximum at $\simeq 225$ K, with a similar frequency dependence to that of sample C. It is important to remark that above $\simeq 250$ K both components of the ac susceptibility are frequency independent within the experimental sensitivity. The intensity of the peak of the real component has an in-

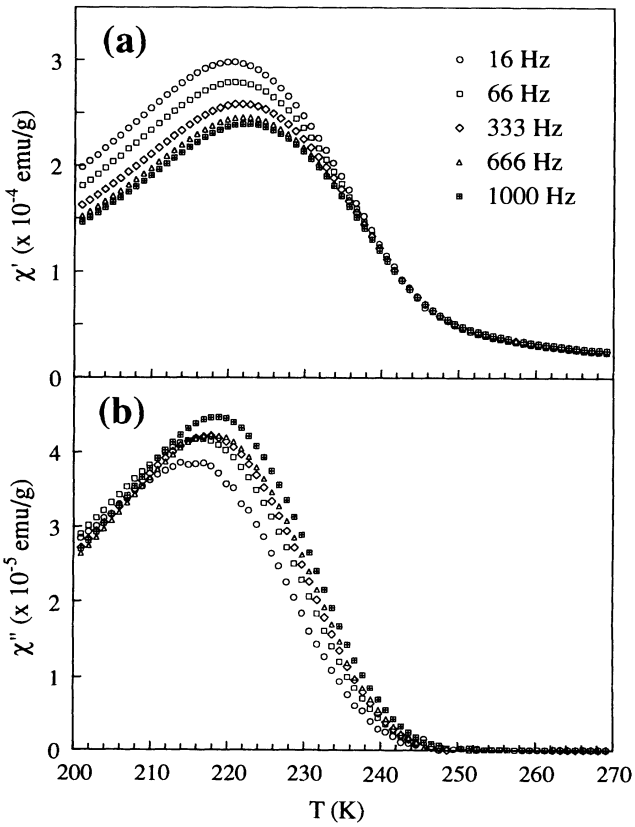

FIG. 8. Real (a) and imaginary (b) parts of the ac susceptibility of sample C, measured with $h_{ac}=5$ Oe and frequencies between 16 and 1000 Hz.

termediate value between samples A and B, and sample C, i.e., $\chi'_{max} \simeq 1.1 \times 10^{-4}$ emu/g.

The ac susceptibility of sample E presents at $\simeq 200$ K the strongest peak of all the measured samples ($\chi'_{max} \simeq 4 \times 10^{-4}$ emu/g). The peaks for both components of the ac susceptibility show a similar frequency dependence to that explained above.

The other four samples (F–I) exhibit a peak of the ac susceptibility similar to that found for samples A and B ($\chi'_{max} \simeq 4 \times 10^{-5}$ emu/g) at $\simeq 257$ K.

We may conclude that the peak of the ac susceptibility ($\chi' \simeq 4 \times 10^{-5}$ emu/g) and the low-field dc magnetization ($M_{dc}/H \simeq 4 \times 10^{-5}$ emu/g) at $T_N = 257(1)$ K is an intrinsic characteristic of Y_2CuO_4. At lower temperatures, an extrinsic contribution to the ac susceptibility and the low-field dc magnetization is observed, which is related to the particular microstructure of the sample. Nevertheless, we should remark that we have not found a clear correlation between this extrinsic behavior of the samples and the pressure of synthesis, which is the only experimental parameter varied for different preparation procedures. For instance, samples made under similar pressure or even different pieces produced in the same synthesis process (samples C and D) exhibited different behavior.

V. DISCUSSION

A. The Néel temperature

The narrow peak of the ac susceptibility and the low-field dc magnetization, found at $T_N = 257(1)$ K for samples A, B, and F–I, has been associated with a transition to a state with three-dimensional (3D) long-range AF order including a WF component (WF phase in Fig. 5).[15] Above T_N, short-range AF correlations of 2D character probably persist (AF1 phase in Fig. 5), as has already been demonstrated for other T' cuprates, based on neutron-scattering experiments.[2–4]

Neutron-scattering measurements have not been performed on Y_2CuO_4 and the synthesis procedure under high pressure has not allowed us to produce large enough single crystals for studying their magnetization parallel and perpendicular to the CuO_2 planes. However, both kinds of experiments have been performed on Gd_2CuO_4 and the structural similarities between both cuprates suggest that the conclusions deduced for the last compound may also apply to Y_2CuO_4. Then, we will assume that the antiferromagnetically ordered Cu moments of Y_2CuO_4 lie in the *ab* planes, similar to Gd_2CuO_4.[9,10] The displacements of the O(1) ions of the CuO_2 planes from a perfect square-planar arrangement, as inferred from x-ray-diffraction experiments for Y_2CuO_4 and Gd_2CuO_4 and from neutron-scattering measurements performed on Gd_2CuO_4,[17,18] suggest that the magnetic moments may be canted away from perfect AF alignment, although remaining in the CuO_2 planes, thus inducing WF components also lying in these planes. The magnetization measurements made in different directions of Gd_2CuO_4 single crystals have confirmed the canting of the Cu spins within the CuO_2 planes and the induced WF components also lying in these planes.[9]

B. Phenomenological free energy

If two sublattice magnetizations, $\mathbf{M}_1$ and $\mathbf{M}_2$, are used to describe the behavior of the magnetic moments in the CuO_2 planes, staggered and uniform magnetizations may be defined as $\mathbf{l} = (\mathbf{M}_1 - \mathbf{M}_2)/2$ and $\mathbf{m} = (\mathbf{M}_1 + \mathbf{M}_2)/2$. The former vector describes the AF component and the last vector represents the WF component. If $|\mathbf{M}_1| = |\mathbf{M}_2|$, $\mathbf{m}$ results always perpendicular to $\mathbf{l}$.

A simple phenomenological free energy may be written in order to describe the magnetic system of a CuO_2 plane including AF and WF interactions. For temperatures close to T_N, the following expression has been proposed by Borovik-Romanov and Ozhogin:[19]

$$\mathcal{F} = A|\mathbf{l}|^2/2 + |\mathbf{m}|^2/(2\chi_0) + \mathbf{D}\cdot(\mathbf{l}\times\mathbf{m}) + Cl^4/4 - \mathbf{m}\cdot\mathbf{H} , \tag{2}$$

where χ_0 is the uniform 2D susceptibility of the CuO_2 planes and $\mathbf{D}\cdot(\mathbf{l}\times\mathbf{m})$ is the Dzyaloshinski-Moriya antisymmetric exchange term. The orientation of $\mathbf{D}$ depends on the symmetry of the Cu-O(1)-Cu exchange bonds. In the case of Y_2CuO_4, $\mathbf{D}$ is expected to be restricted to the *c* axis due to the in-plane local distortions of the T' structure proposed from x-ray-diffraction experiments.[17] In this case, the energy is lowered by inducing a WF component in the *ab* plane. Similar structural distortions have been found for Gd_2CuO_4 in Ref. 18 and the WF component has been measured in the *ab* plane as expected.[9]

If $\mathbf{H}$ is applied perpendicular to $\mathbf{D}$, then $\mathbf{m}$ is parallel to $\mathbf{H}$, χ_0 is the uniform 2D susceptibility parallel to the *ab* planes and $\mathbf{m}$, $\mathbf{l}$, and $\mathbf{D}$ are mutually perpendicular. Using a reference system where $\mathbf{m} = mx$, $\mathbf{l} = ly$, and $\mathbf{D} = Dz$, the equilibrium conditions $\partial\mathcal{F}/\partial m = \partial\mathcal{F}/\partial l = 0$ lead to the equations

$$\begin{aligned} &m = \chi_0(H + Dl) , \\ &Cl^3 + [A(T) - \chi_0 D^2]l - \chi_0 DH = 0 . \end{aligned} \tag{3}$$

When $T > T_N$, only a residual AF order persists and the Cl^3 term may be neglected. On the other hand, when $T < T_N$, Eq. (3) may be solved using the perturbation approach $|l(H,T)| = l_0(T) + a_1(T)H + a_3(T)H^3 + \cdots$, where $l_0(T) = (\nu/C)^{1/2}(T_N - T)^{1/2}$ corresponds to the solution for $H = 0$ and $T < T_N$.[15,19] In this expression, T_N is the Néel temperature determined from the condition $\nu(T - T_N) = A(T) - \chi_0 D^2 < 0$. For $T > T_N$, only the trivial solution $l_0(T) = 0$ is possible.

Thus, for $H \neq 0$, we obtain

$$m = \begin{cases} \chi_0[1 + D^2\chi_0/\nu(T - T_N)]H + O(H^3), & T > T_N \\ \chi_0 D l_0(T) + \chi_0[1 + D^2\chi_0/2\nu(T_N - T)]H \\ \quad + O(H^3), & T < T_N . \end{cases} \tag{4}$$

A comparison with Eq. (1) indicates that, for low applied fields,

$$M_S(T)=\chi_0 D l_0(T)=\chi_0 D(\nu/C)^{1/2}(T_N-T)^{1/2}$$

for $T\leq T_N$ and $M_S(T)=0$ for $T\geq T_N$.

Above T_N, the low-field differential susceptibility is given by $\chi_d(T)=\chi_0+(D\chi_0)^2/\nu(T-T_N)$. A fit of $\chi_d(T)$ for sample A at temperatures close above T_N gives

$$\chi_d=\chi_0+(D\chi_0)^2\nu^{-1}(T-T_N)^{-\gamma} \quad (5)$$

with $\gamma=1.10(9)$. As shown in the inset of Fig. 1(a), the quality of the fit is excellent for $T>265$ K. From this fit, we have determined $\chi_0=1.4(5)\times10^{-6}$ emu/g and $(D\chi_0)^2/\nu=1.8(2)\times10^{-4}$ K emu/g. The value $\chi_0=1.4(5)\times10^{-6}$ emu/g$=4.3(1.5)\times10^{-4}$ emu/mol corresponds to the powder average of the uniform 2D susceptibility of Eq. (2). Within the framework of the $\frac{1}{2}$-Heisenberg antiferromagnetic model on a square-planar lattice, a theoretical value may be calculated from the zero-temperature expression $\chi=(g\mu_B)^2/(8J_\parallel)$.[20] We have used the magnitude $J_\parallel=1400$ K, found for the cuprates R_2CuO_4, with $R=$Pr, Nd, and Sm,[2-4] and we have made a powder average of the calculated χ_0, keeping in mind that, for Y_2CuO_4, it corresponds to a parallel susceptibility of the CuO_2 planes. Using an anisotropy $\chi_0^{ab}/\chi_0^c\geq3.5$, larger than that found for La_2CuO_4,[21] we have calculated a value $\chi_0^{\text{powder}}\simeq0.9$ emu/mol, smaller by a factor $\simeq5$ than our experimental determination. The experimental susceptibility of La_2CuO_4, after being powder averaged, $\chi_0\simeq1.2$ emu/mol,[20] is also larger than its calculated value, but smaller than the Y_2CuO_4 estimation by a factor $\simeq3.5$. The large value we have found may be attributed to the in-plane distortions of the Y_2CuO_4 compound, which break the square-planar coordination and enhance the WF component.

From the high-field magnetization data at low temperatures, we have extrapolated $M_S(0)\simeq0.17$ emu/g$=9.3\times10^{-3}\mu_B$/Cu atom for sample A and $M_S(0)\simeq0.21$ emu/g$=11.5\times10^{-3}\mu_B$/Cu atom for sample C. Assuming a classical spin model at zero temperature, the ratio between the WF component of the Cu moments, $M_S(0)$, and the staggered magnetization, $l_0(0)=g\mu_B S$, gives an estimate for the canting angle Θ:

$$\Theta=\tan^{-1}[|m(0)|/|1(0)|]=\tan^{-1}[M_S(0)/l_0(0)]$$
$$=\tan^{-1}D\chi_0 . \quad (6)$$

Using the moment measured for R_2CuO_4 with $R=$Pr, Nd, and Sm, $l_0(0)=0.4(1)\mu_B$/Cu atom,[2-4] in this expression, we obtain $\Theta=1.3(3)°$ for sample A and a rather similar value for sample C [$\Theta=1.6(3)°$].

The magnetic moment associated with the spin $S=\frac{1}{2}$ of the Cu ions is expected to be reduced due to the two dimensionality of the system by a factor b, so that

$$l_0(0)=g\mu_B bS . \quad (7)$$

A reduction factor $b=0.606$ has been proposed from spin-wave theory for the $\frac{1}{2}$-Heisenberg antiferromagnet on a 2D square lattice.[20] Using $g=2$, this value of the reduction factor predicts $l_0(0)=0.61\mu_B$/Cu atom, which is larger than the moment measured for R_2CuO_4 with $R=$Pr, Nd, and Sm, $l_0(0)=0.4(1)\mu_B$/Cu atom. As we use this latter value in our calculation, the corresponding reduction factor should be $b\simeq0.4$.

From the value of $D\chi_0$ for sample A, calculated from Eq. (6), and the value of $(D\chi_0)^2/\nu$, determined from the fit of χ_d to Eq. (5), we obtain $\nu^{-1}=0.4(2)$ K emu/g$=130(65)$ K emu/mol. This parameter is related to the staggered susceptibility of the system, which in a mean-field approximation is given by $\chi^\dagger=C_m/(T-T_N)$, where C_m is the Curie constant of the AF species and, thus, $\nu^{-1}=C_m$. This value obtained for Y_2CuO_4 may be compared with $\nu^{-1}\simeq350$ K emu/mol for Gd_2CuO_4.[22]

The measured parameters may be related to the exchange Hamiltonian that describes the in-plane magnetic interactions,

$$H_{\text{ex}}=\sum_{\langle i,j\rangle} S_i J S_j-g\mu_B\sum_i S_i H , \quad (8)$$

where

$$J=\begin{bmatrix} J^{aa} & J^{ab} & 0 \\ -J^{ab} & J^{bb} & 0 \\ 0 & 0 & J^{cc} \end{bmatrix} .$$

The average interaction is AF with $J_\parallel=(J^{aa}+J^{bb}+J^{cc})/3$. We have assumed that all the spins lie in the ab plane and this implies that $|J^{cc}|$ is the smallest of the diagonal terms.

Because of the antisymmetric coupling J^{ab}, the spins are canted away from perfect AF order by an angle Θ which, on the average, is given by

$$\tan\Theta=\langle J^{ab}\rangle/(2J_\parallel) . \quad (9)$$

If we assume for the $J_\parallel$ of Y_2CuO_4 the same value found for the cuprates R_2CuO_4 ($R=$Pr, Nd, and Sm), i.e., $J_\parallel\simeq1400$ K,[2-4] we determine an average value $\langle J^{ab}\rangle\simeq65$ K for sample A and a quite similar value for sample C.

C. The metamagnetic transition

When a magnetic field is applied, the competition between the Zeeman energy in Eq. (8) and the interlayer AF coupling should be considered. The low values of $M_{\text{dc}}(H,T)$ below H_c, measured for sample A, indicate that the WF components in neighboring planes are oriented antiferromagnetically and a 3D AF order eventually exists because of the interlayer coupling $J_\perp$ (AF2 phase in Fig. 5). At $T=0$ and $H=H_c$ applied on the CuO_2 planes, the WF component of each plane points in the direction of the field and this implies an energy gain for the system of $M_S(0)H_c(0)$. However, to reach this state, the inversion of the WF component of half of the CuO_2 planes has to take place. For this inversion, a full reversal of the spins in these planes is necessary, with an energy loss of $4J_\perp(bS)^2$. The energy balance let us estimate a value for the interlayer coupling constant, through the expression[16]

$$J_\perp=M_S(0)H_c(0)/(4b^2S^2) . \quad (10)$$

In the metamagnetic transition, two different values for the critical field, H_c' and H_c'', have been found depending on whether we increase or decrease the field, respectively. Both critical fields coincide above a tricritical temperature, T_t, located at $\simeq 240$ K. The hysteretic behavior is a typical feature of metamagnetic transitions and is mainly due to the internal field produced by the ferromagnetically ordered component of the spins.[23,24] However, in the present case, the hysteresis is not only due to the metamagnetic transition, but it is enhanced by the underlying structural distortion of the sample, which will be analyzed in Sec. V E. The magnetic phase between $H_c'(T)$ and $H_c''(T)$ has been called M phase (mixed phase) in Fig. 5 for analogy with the typical metamagnetic transitions. The enhancement of the hysteresis, especially at low temperatures, makes difficult the determination of the internal critical field. At 5 K, H_c' has been measured for sample A from the first magnetization curve and its value is $\simeq 4$ kOe; the values of H_c'' below 130 K are negative and they cannot be measured. Using $H_c(0) \simeq 4$ kOe and the $M_S(0)$ of sample A in Eq. (10), we estimate $J_\perp \simeq 17$ mK. Thus, using again $J_\parallel \simeq 1400$ K for the Y_2CuO_4, the ratio between interlayer and intralayer coupling is about 1.2×10^{-5}, of the same order as that found for La_2CuO_4.[16]

A determination of the critical exponents of the metamagnetic transition is complex because of the difficult calculation of the internal field and the small magnitude of the differential susceptibility. Nevertheless, we have determined the tricritical exponent α' for sample A by fitting below T_t the differential susceptibility, measured at the tricritical field $H_t \simeq 600$ Oe, to the expression

$$\chi_d(H_t,T) = A(T_t - T)^{-\alpha'} . \quad (11)$$

In this equation, the derivative $\chi_d \equiv \partial M_{dc}/\partial H$ has to be obtained with respect to the internal field, $H_i = H - NM$, where H is the applied field and N is the demagnetization factor. We have obtained $\alpha' = 0.51(2)$, a value close to that expected from mean-field theory.[23]

For sample C, the situation below the critical line, $H_c(T)$, is quite different. In this case, the isothermal magnetization vs field measurements show that a ferromagnetic component persists even below the critical field (see Fig. 6). However, the value of the extrapolated saturation magnetization at 0 K in this regime [$M_S(0) \simeq 1.3 \times 10^{-3} \mu_B$/Cu atom] is about nine times smaller than its value in the WF state above H_c [$M_S(0) \simeq 11.5 \times 10^{-3} \mu_B$/Cu atom]. This behavior indicates that the WF components are not totally compensated below H_c. We may assume that some clusters of the sample, about 10%, which are specially disordered, cannot undergo the metamagnetic transition and remain in a WF state. The behavior of this percentage of clusters partially masks the metamagnetic transition exhibited by the rest of them. The critical field measured at 5 K for increasing fields [$H_c'(5\text{ K}) \simeq 5$ kOe] is not very different from that of sample A and the critical field measured for decreasing fields, H_c'', is also negative. The same arguments given at the beginning of this section to explain the metamagnetic transition of sample A may be applied to sample C, although, in this case, some clusters still remain ferromagnetically ordered below H_c. Equation (10) also may be used and gives a value of $J_\perp$ slightly larger for sample C, due to higher values of $M_S(0)$ and $H_c(0)$. We have estimated the last parameter to be $H_c(0) \simeq 5$ kOe.

D. The weak ferromagnetic transition

A surprising observation is that the ferromagnetic (FM) behavior of both samples A and C, as indicated by the values of $M_S(T)$, is present up to temperatures $\simeq 300$ K, well above T_N. A similar behavior has also been found for Gd_2CuO_4, where the dc magnetization measurements and the electron-spin-resonance signal of the Gd ions indicated the persistence of a WF component of the Cu moments up to $\simeq 50$ K above T_N.[22]

A characteristic temperature of a FM system in an applied magnetic field is that of the inflexion point of M_{dc} vs T. The minimum of the $\partial M_{dc}(T)/\partial T$ curves in Fig. 9(a) clearly signals this point for sample A.

Another typical characteristic of the behavior of the FM transition is the peak of $\chi_d(H,T)$ vs T for a given field, which typically shifts towards higher temperatures on increasing field.[25] In Fig. 9(b), we show a strong peak in sample A for low fields. When the field is increased, this peak becomes weaker and shifts towards higher temperatures.

In Fig. 10, we plot with open squares the inflexion points of the magnetization vs temperature of sample A

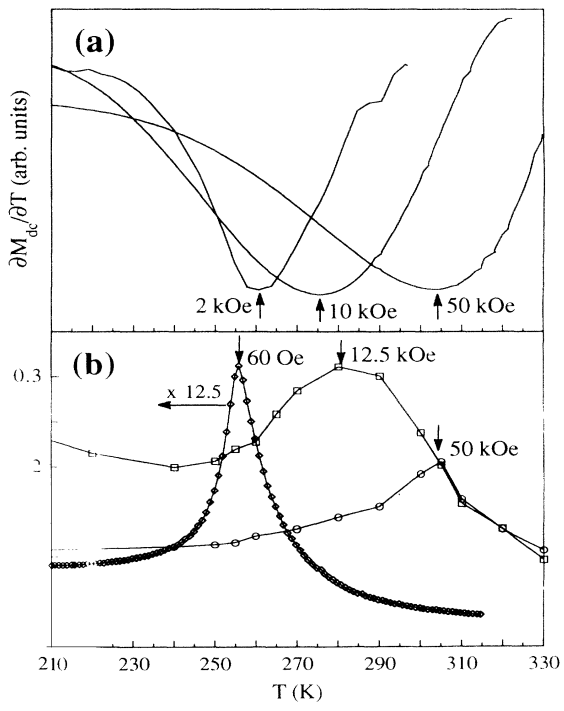

FIG. 9. (a) Derivative of the dc magnetization with temperature for sample A and fields of 2, 10, and 50 kOe. (b) Differential susceptibility versus temperature of sample A at 60 Oe, 12.5, and 50 kOe. In both cases, the arrows indicate the maxima which define the points of the WF transition.

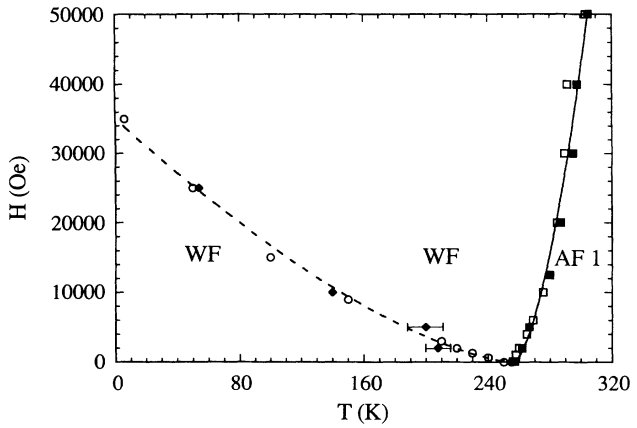

FIG. 10. Phase diagram of sample A of Y_2CuO_4 at high magnetic fields. Open squares are the inflexion points of the $M_{dc}(T)$ curves, full squares are the maximum of the $\chi_d(T)$ curves, and the solid line is a fit to the function $H=H_0(T/T_N-1)^{\gamma+\beta}$. Circles are the irreversibility points of the $M_{dc}(H)$ cycles and the dotted line is a fit to the law $H=H_0(1-T/T_N)^{3/2}$. The irreversibility points of sample C are also plotted as full diamonds.

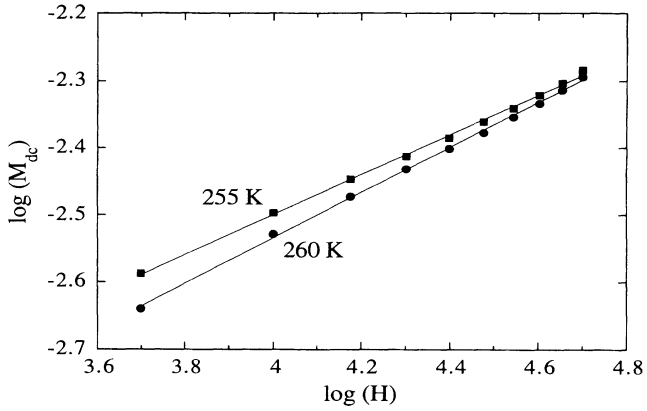

FIG. 11. Isothermal magnetization vs field plotted with logarithmic axes to base 10 around the Néel temperature, $T_N \simeq 257$ K, for sample A. The lines display the power law $M_{dc}=AH^{1/\delta}$ with $\delta=3.15(20)$.

and with full squares the maximum of the differential susceptibility peaks at different fields. These points separate two different phases (AF1 and WF) in the phase diagram of Fig. 10 and can be fitted to the same function

$$H/H_0=[T(H)/T_c-1]^{\gamma+\beta} \tag{12}$$

with $T_c=T_N=257$ K. From this fit, we obtain the parameters $(\gamma+\beta)=1.7(2)$ and $H_0=870(300)$ kOe. This kind of function can be deduced from a scaling-law equation of state which, in the vicinity of the ferromagnetic critical temperature, has the form $m(h,t)=t^{\beta}F(h/t^{(\gamma+\beta)})$ where m, h, and $t=|(T-T_N)/T_N|$ are reduced variables.[26] This equation leads to the well-known asymptotic behavior

$$m(h=0,t)\propto t^{\beta}, \quad T<T_N \tag{13}$$

$$\chi(h=0,t)\propto t^{-\gamma}, \quad T>T_N \tag{14}$$

$$m(h,t=0)\propto h^{1/\delta} . \tag{15}$$

Fitting the low-field differential susceptibility above the peak to Eq. (7), which is equivalent to Eq. (14), we have determined $\gamma=1.10(9)$. From the fit of the isothermal magnetization vs field at temperatures around T_N to Eq. (15) (Fig. 11), we have found $\delta=3.15(20)$. We cannot use Eq. (13) because of the metamagnetic transition which masks $m(h=0,t)$ below T_N. But we can calculate β from the relations $\Delta=\gamma+\beta=\beta\delta$, knowing $\gamma+\beta$ from Eq. (12) and the other two critical exponents. From $\Delta=\gamma+\beta$ and $\gamma=1.10(9)$, we obtain $\beta=0.56(29)$. From $\Delta=\beta\delta$ with $\delta=3.15(20)$, we obtain $\beta=0.53(10)$, in close agreement with the previous value. In all cases, the exponents found are close to those expected from mean-field theory.[26]

We have also determined the WF transition of sample C from the inflexion points of the $M_{dc}(T)$ curves at different fields. The critical behavior of this transition is very similar to that of sample A, with a coincident critical exponent $\Delta=(\gamma+\beta)=1.8(3)$.

E. ac dynamics and relaxation effects

The peak of the ac susceptibility at $T_N \simeq 257$ K for sample B does not show any detectable frequency dependence, in accordance with a well-behaved antiferromagnetic transition. On the other hand, the susceptibility peaks observed at lower temperatures, $\simeq 220$ K for samples C and D and $\simeq 190$ K for sample E, show a strong frequency dependence more characteristic of a spin-glass or cluster freezing behavior (see Fig. 8), with the freezing temperature signaled by the maximum of the susceptibility.

There are basically two different possible interpretations of the spin-glass freezing: One assumes the existence of a true equilibrium phase transition at finite temperature and is commonly accepted for canonical spin glasses.[27] The other interpretation assumes the existence of clusters and, in this case, the freezing is a nonequilibrium phenomenon.[28] For isolated clusters, the frequency dependence of their blocking temperature has been predicted, according to the Néel model,[29] to follow an Arrhenius law

$$\tau=\tau_0\exp(E_a/kT_B) , \tag{16}$$

where E_a is the potential barrier which separates two easy orientations of the cluster. For magnetically interacting clusters, instead a Vogel-Fulcher law has been proposed:

$$\tau=\tau_0\exp[E_a/k(T_B-T_0)] , \tag{17}$$

where T_0 can be viewed as a phenomenological parameter which describes the intercluster interaction. Equation (17) is only valid for $T_B \gg T_0$ and implies a linear dependence of the blocking temperature, T_B, on the magnitude $1/\ln(2\pi\nu\tau_0)^{-1}$. We have found a good fit to this linear

dependence in sample C, for all the measured frequency range (10–1000 Hz) using the value $\tau_0=10^{-12}$ s. From this fit, we have also determined $T_0\simeq 200$ K.

Recently, there have been attempts to describe the dynamic properties of the spin glasses within the framework of critical phenomena associated with a transition. The scaling laws have been proposed for the critical slowing down of the relaxation time. The $T_c\neq 0$ transition model predicts a power law,[30]

$$\tau=\tau_0[T_f/(T_f-T^*)]^{\alpha}\ , \tag{18}$$

which leads to a scaling of $\chi''(T,\omega)$ by using the relation

$$\chi''(T,\omega)=t^{\beta}G(\omega\tau)\ , \tag{19}$$

where $G(x)$ is a universal function of x, $t=(T-T_c)/T_c$ is the zero-field-reduced temperature, and β is the exponent of the order parameter.

Activated dynamics have been also proposed to explain the observance of a cusp in the $\chi'(T)$ curve. In this case, a set of interacting superparamagnetic clusters has a finite probability to overcome an energy barrier, E_α, which scales with the correlation length ξ, $E_\alpha\propto\xi^{\theta}$, and, if a generalized Arrhenius law holds for the relaxation time,[31] we have

$$\ln(\tau/\tau_0)\propto\xi^{\theta}\propto(T-T_{\mathbf{B}})^{-\nu\theta}\ . \tag{20}$$

Near $T_{\mathbf{B}}$, the scaling relationship characteristic of activated dynamics may be written as

$$\chi''(T,\omega)=t^{P}G[-t^{Q}\ln(\omega\tau_0)]\ , \tag{21}$$

where $G(x)$ is again a universal function of x and P and Q are critical exponents.

We have found it impossible to obtain a good scaling of the experimental data of sample C, for any reasonable value of the parameters, to the power function scaling (19), characteristic of spin glasses with transition at a finite temperature. Instead, an excellent scaling was obtained using the expression (21) with $T_c=215.5$ K, $P=1.4$, $Q=0.55$, and the value $\tau_0=10^{-12}$ s obtained from the Vogel-Fulcher plot (inset of Fig. 12). The quality of this scaling is shown in Fig. 12. Despite the nonuniversality of the P and Q exponents, indicative of significant differences between the dynamic behavior and the relaxation processes of each system, the values that we have found are similar to those reported for other materials described as systems of interacting clusters.[32]

Closely related to the dynamic behavior of frozen interacting clusters is the observation of irreversibility in the $M_{\mathrm{dc}}(H,T)$ vs T measurements, depending on ZFC and FC procedures.[33] This irreversibility is also observed as a hysteresis in the $M_{\mathrm{dc}}(H,T)$ vs H curves at different temperatures. The line that delimits the reversible region in the H-T diagrams has been well determined for sample A (Fig. 10). The irreversibility line follows the equation

$$H_{\mathrm{irr}}/H_0=(1-T/T_c)^{3/2} \tag{22}$$

as a de Almeida–Thouless line. The $h^{3/2}$ dependence is typically exhibited by the freezing temperature of spin glasses and the blocking temperature of systems of interacting clusters.[34] We have also determined some irreversibility points for sample C and we have found an absolute coincidence with those determined for sample A.

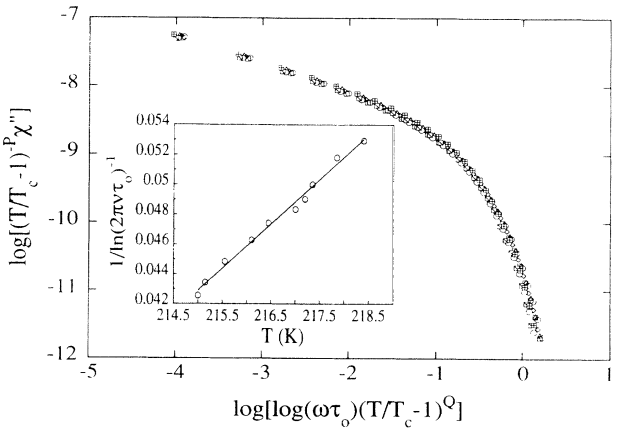

FIG. 12. Activated dynamic scaling $\chi''=t^{P}G[-\ln(\omega\tau_0)t^{Q}]$, with $t=T/T_c-1$ ($T_c=215.5$ K), $P=1.4$, $Q=0.55$, and $\tau_0=10^{-12}$ s, for seven sets of measurements of sample C with $h_{\mathrm{ac}}=5$ Oe and frequencies between 16 and 1000 Hz. Inset: Variation of the temperature of the maximum of the imaginary part of the ac susceptibility with the frequency of the ac field ($h_{\mathrm{ac}}=5$ Oe), in a Vogel-Fulcher plot for sample C. From the linearity of this plot we obtain $\tau_0=10^{-12}$ s.

In order to verify that the observed irreversibility line really corresponds to a blocking of weak ferromagnetic clusters, we have measured the magnetization relaxation after the ZFC process for sample C at two different fields, below and above this line. As expected, the magnetization measured at 110 K and 500 Oe, i.e., in the irreversible region, shows the dependence $M_{\mathrm{dc}}(t)\propto\ln(t)$ (Fig. 13), characteristic of spin-glass or interacting-cluster systems.[28,35] Above the irreversibility line, at 110 K and 25 000 Oe, the time dependence of the ZFC magnetization is negligible.

The microscopic origin of the weak ferromagnetic clusters responsible of the observed dynamics in the Y_2CuO_4 cuprates is not clearly ascertained. However, it is very

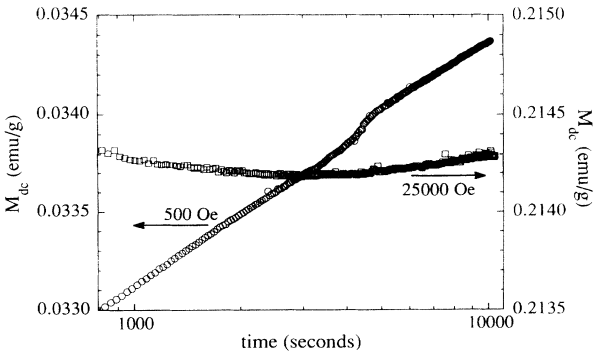

FIG. 13. Magnetization relaxation after ZFC for sample C, at 110 K, below the irreversibility line ($H=500$ Oe, circles) and above it ($H=25\,000$ Oe, squares). Notice that both y-axis scales are the same.

likely that the crystallographic distortion of the tetragonal T' structure allowing the development of a WF component has no long-range order. This would lead to finite-size weak ferromagnetic clusters depending on the detailed microstructure of the samples. The differences in the microstructure of the samples investigated lead to strongly modified behaviors concerning the low-temperature peak associated to the freezing of these finite-size clusters. So, we may conclude that while T_N is an intrinsic characteristic of all the Y_2CuO_4 samples, the freezing phenomenon is more extrinsic, depending on the relevance and extent of the local structural distortion leading to the observed lattice superstructures.

VI. CONCLUSIONS

The peak of the ac susceptibility and the low-field dc magnetization found at 257(1) K for most of the samples determines the Néel temperature, T_N. This temperature signals the transition of the Cu lattice to long-range 3D AF order. The ordered Cu spins lie in the CuO_2 planes and, above T_N, short-range AF correlations of 2D character probably persist.

The T' structure of Y_2CuO_4 is affected by local distortions, which break the Cu-O square-planar coordination. Then, a Dzyaloshinski-Moriya antisymmetric exchange term is allowed in the Hamiltonian of the system. The antisymmetric exchange coupling produces a canting of the Cu spins away from perfect AF alignment, but still lying on the CuO_2 planes. As a consequence, a WF component within the CuO_2 planes is induced. Assuming for Y_2CuO_4 the same intraplanar coupling constant, $J_{\parallel} \simeq 1400$ K, and the same staggered magnetization, $l_0(0)=0.4\mu_B$/Cu atom, found for other cuprates of the same structure, we estimate for sample A an average antisymmetric exchange coupling constant around $\langle J^{ab} \rangle \simeq 65$ K and a canting angle around $\Theta \simeq 1.3°$. The behavior of sample A is also exhibited by most of the Y_2CuO_4 samples and its estimated parameters are rather similar to those obtained from sample C, which presents some different behaviors. Consequently, we assume that these parameters are intrinsic and universal for the Y_2CuO_4 cuprates.

At zero field below T_N, the AF interlayer coupling orients the WF components in neighboring planes antiferromagnetically. This order holds until a metamagneticlike transition occurs. For fields above this transition, the Zeeman energy overcomes the energy of the AF interlayer coupling and, then, a typical WF phase appears unmasked. From sample A, we have estimated the AF interlayer coupling constant around $J_{\perp} \simeq 17$ mK, the critical field where the metamagnetic transition takes place at 0 K around $H_c(0) \simeq 4$ kOe and the extrapolated saturation magnetization reached by the WF component about $M_S(0) \simeq 9.3 \times 10^{-3} \mu_B$/Cu atom. Above T_N, the WF phase still persists induced by the field. The transition from this phase to the high-temperature paramagnetic phase with short-range 2D AF correlations is given by the function $h=t^{(\gamma+\beta)}$, where $h=H/H_0$ and $t=(T-T_N)/T_N$. The critical exponents found for both the metamagnetic transition and the WF transition are close to those expected from mean-field theory.

Nevertheless, this system exhibits some properties, such as enhanced hysteresis loops, an irreversibility line (IL), relaxation effects below this IL, and some frequency dependence of the ac susceptibility below $T_N \simeq 257$ K, which cannot be explained in the scope of the theory of weak ferromagnetism of ordered materials. These features are more characteristic of disordered magnetic systems, so, to explain them, we have assumed that there is an inhomogeneous distribution of the local structural distortions allowing the weak ferromagnetic behavior. This inhomogeneous distribution leads to finite-size weak ferromagnetic clusters depending on the detailed microstructure of the samples. The differences in the microstructure of different samples produce strongly modified behaviors concerning the appearance of a low-temperature peak in the ac susceptibility associated to the freezing of the finite-size clusters. This peak displays a strong frequency dependence, while that corresponding to T_N was found to be independent of the frequency. The imaginary component of the ac susceptibility measured at different frequencies may be well scaled to the activated dynamic relation $\chi''=t^P G[-t^Q \ln(\omega\tau_0)]$, which is characteristic of systems of interacting clusters. Related to this behavior, a universal irreversibility line has been determined, which follows a de Almeida–Thouless-like law $t \propto h^{2/3}$, and logarithmic relaxation processes have been observed below it.

All these features have led us to observe a complex magnetic phase diagram for the Y_2CuO_4 cuprates, where the intrinsic microscopic magnetic interactions, producing the long-range AF order at T_N, the weak ferromagnetic phase and the metamagnetic transition, combine with a more extrinsic distribution of local structural distortions, which leads to finite-size WF interacting clusters.

ACKNOWLEDGMENTS

We are indebted to Dr. B. Martínez for helpful discussions. Financial support received from the Spanish Dirección General de Investigación en Ciencia y Tecnología (PB 92-0849) and the EEC (CT92-0087 and CT92-0785) is also acknowledged.

[1] Y. Tokura, H. Takagi, and S. Uchida, Nature (London) **377**, 345 (1989); H. Takagi, S. Uchida, and Y. Tokura, Phys. Rev. Lett. **62**, 1197 (1989).

[2] S. Skanthakumar, H. Zhang, T. W. Clinton, W.-H. Li, J. W. Lynn, Z. Fisk, and S.-W. Cheong, Physica C **160**, 124 (1989).

[3] M. Matsuda, K. Yamada, K. Kakurai, H. Kadowski, T. R. Thurston, Y. Endoh, Y. Hidaka, R. J. Birgeneau, M. A. Kastner, P. M. Gehring, A. H. Moudden, and G. Shirane, Phys. Rev. B **42**, 10 098 (1990).

[4] S. Skanthakumar, J. W. Lynn, J. L. Peng, and Z. Y. Li, J. Appl. Phys. **69**, 4866 (1991).

[5] A. S. Cherny, E. N. Khats'ko, G. Chouteau, J. M. Louis, A. A. Stepanov, P. Wyder, S. N. Barilo, and D. I. Zhigunov, Phys. Rev. B **45**, 12 600 (1992).

[6]S. Skanthakumar, J. W. Lynn, J. L. Peng, and Z. Y. Li, Phys. Rev. B **47**, 6173 (1993).

[7]M. B. Maple, N. Y. Ayoub, J. Beille, T. Bjornholm, Y. Dalichaouch, E. A. Early, S. Ghamaty, B. W. Lee, J. T. Markert, J. J. Neumeier, G. Nieva, L. M. Paulius, I. K. Schuller, C. L. Seaman, and P. K. Tsai, *Proceedings of the International Conference on Transport Properties of Superconductors (ICTPS'90),* Progress in High-Temperature Superconductivity Vol. 25, edited by R. Nickolsky (World Scientific, Singapore, 1990), p. 536.

[8]A. Butera, A. Caneiro, M. T. Causa, L. B. Steren, R. Zysler, M. Tovar, and S. B. Oseroff, Physica C **160**, 341 (1989).

[9]S. B. Oseroff, D. Rao, F. Wright, D. C. Vier, S. Schultz, J. D. Thompson, Z. Fisk, S.-W. Cheong, M. F. Hundley, and M. Tovar, Phys. Rev. B **41**, 1934 (1990).

[10]T. Chattopadhyay, P. J. Brown, B. Roessli, A. A. Stepanov, S. N. Barilo, and D. I. Zhigunov, Phys. Rev. B **46**, 5731 (1992).

[11]I. E. Dzyaloshinski, Zh. Eksp. Teor. Fiz. **32**, 1547 (1957) [Sov. Phys. JETP **5**, 159 (1957)]; T. Moriya, *Magnetism,* edited by G. T. Rado and H. Suhl (Academic, New York, 1966), Vol. 1, p. 85.

[12]H. Okada, M. Takano, and Y. Takeda, Phys. Rev. B **42**, 6813 (1990); M. Tovar, X. Obradors, F. Pérez, S. B. Oseroff, R. J. Duro, J. Rivas, D. Chateigner, P. Bordet, and J. Chenevas, *ibid.* **45**, 4729 (1992).

[13]C. Lin, G. Lu, Z.-X. Liu, and Y.-F. Zhang, Physica C **194**, 66 (1992); Solid State Commun. **84**, 721 (1992).

[14]B. Büchner, M. Cramm, M. Braden, W. Braunisch, O. Hoffels, W. Schnelle, R. Müller, A. Freimuth, W. Schlabitz, G. Heger, D. I. Khomskii, and D. Wohlleben, Europhys. Lett. **21**, 953 (1993); M. K. Crawford, R. L. Harlow, E. M. McCarron, W. E. Farneth, J. D. Axe, H. Chou, and Q. Huang, Phys. Rev. B **44**, 7749 (1991).

[15]A. Rouco, X. Obradors, M. Tovar, P. Bordet, D. Chateigner, and J. Chenavas, Europhys. Lett. **20**, 651 (1992).

[16]S.-W. Cheong, J. D. Thompson, and Z. Fisk, Phys. Rev. B **39**, 4395 (1989).

[17]P. Bordet, J. J. Capponi, C. Chaillout, D. Chateigner, J. Chenavas, Th. Fournier, J. L. Hodeau, M. Marezio, M. Perroux, G. Thomas, and A. Varela-Losada, Physica C **193**, 178 (1992).

[18]Ph. Galez, P. Schweiss, G. Collin, and R. Bellisend, J. Less-Common Met. **164&165**, 784 (1990); M. Braden, W. Paulus, A. Cousson, P. Vigoureux, G. Heger, A. Gukasov, P. Bourges, and D. Petitgrand, Europhys. Lett. **25**, 625 (1994).

[19]A. S. Borovik-Romanov and V. I. Ozhogin, Zh. Eksp. Teor. Fiz. **39**, 27 (1960) [Sov. Phys. JETP **12**, 18 (1961)].

[20]E. Manousakis, Rev. Mod. Phys. **63**, 1 (1991); T. Thio, T. R. Thurston, N. W. Preyer, M. A. Kastner, H. P. Jenssen, D. R. Gabbe, C. Y. Chen, R. J. Birgeneau, and A. Aharony, Phys. Rev. B **38**, 905 (1988).

[21]W. C. Lee and D. C. Johnston, Phys. Rev. B **41**, 1904 (1990), and references therein.

[22]L. B. Steren, A. Fainstein, M. Tovar, A. Rouco, F. Pérez, X. Obradors, J. Mira, J. Rivas, S. B. Oseroff, and Z. Fisk, J. Appl. Phys. **73**, 5710 (1993).

[23]E. Stryjewski and N. Giordano, Adv. Phys. **26**, 487 (1977).

[24]E. Yi Chen, J. F. Dillon, Jr., and H. J. Guggenhein, in *Magnetism and Magnetic Materials,* edited by C. D. Graham and J. J. Rhyne, AIP Conf. Proc. No. 18 (AIP, New York, 1974), p. 329; J. A. Griffin, S. E. Schnatterly, Y. Farge, M. Regis, and M. P. Fontana, Phys. Rev. B **10**, 1960 (1974).

[25]P. Gaunt, S. C. Ho, G. Williams, and R. W. Cochrane, Phys. Rev. B **23**, 251 (1981); J. A. Geohegan and S. M. Bhagat, J. Magn. Magn. Mater. **25**, 17 (1981), and references therein.

[26]S. N. Kaul, J. Magn. Magn. Mater. **53**, 5 (1985).

[27]E. A. Edwards and P. W. Anderson, J. Phys. F **5**, 965 (1975).

[28]J. L. Tholence and R. Tournier, J. Phys. (Paris) Colloq. **35**, C4-229 (1974).

[29]L. Néel, Ann. Geophys. **5**, 99 (1949).

[30]P. C. Hohenberg and B. I. Halperin, Rev. Mod. Phys. **49**, 435 (1977); N. Bontemps, J. Rajchenbach, R. V. Chamberlin, and R. Orbach, Phys. Rev. B **30**, 6514 (1984).

[31]K. Binder and A. P. Young, Phys. Rev. B **29**, 2864 (1984).

[32]B. Martínez, F. Sandiumenge, I. Golosovski, S. Galí, A. Labarta, and X. Obradors, Phys. Rev. B **48**, 16 440 (1993); S. Geschwind, A. T. Ogielski, G. Devlin, and J. Hegarty, J. Appl. Phys. **63**, 3291 (1988); P. Nordblat, L. Lundgren, and P. Svedlingh, J. Phys. (Paris) Colloq. **49**, C8-1069 (1988).

[33]S. Nagata, P. H. Keesom, and H. R. Harrison, Phys. Rev. B **19**, 1633 (1979).

[34]J. R. L. de Almeida and D. J. Thouless, J. Phys. A **11**, 983 (1978); R. V. Chamberlin, M. Hardiman, L. A. Turkevitch, and R. Orbach, Phys. Rev. B **25**, 672 (1982); P. Monod and H. Bouchiad, J. Phys. Lett. **43**, L45 (1982); L. E. Wenger and J. A. Mydosh, Phys. Rev. B **29**, 4156 (1984); J. L. Dormann, D. Fiorani, and M. El Yamani, Phys. Lett. A **120**, 95 (1987).

[35]R. Tournier and Y. Ishikawa, Phys. Lett. **11**, 280 (1964); C. N. Guy, J. Phys. F **5**, L242 (1975).